ACS APPLIED MATERIALS & INTERFACES

Research Article

Cite This: ACS Appl. Mater. Interfaces 2017, 9, 43478−43489

www.acsami.org

High-Performance Poly(lactic-co-glycolic acid)-Magnetic Microspheres Prepared by Rotating Membrane Emulsification for Transcatheter Arterial Embolization and Magnetic Ablation in VX_2 Liver Tumors

Yi-Jun Liang,[†,§,∥] Hui Yu,[‡,∥] Guodong Feng,[‡,∥] Linlin Zhuang,[†] Wei Xi,[‡] Ming Ma,[†,§] Jun Chen,[*,‡] Ning Gu,[*,†,§] and Yu Zhang[*,†,§]

[†]State Key Laboratory of Bioelectronics, Jiangsu Key Laboratory for Biomaterials and Devices, School of Biological Science and Medical Engineering, Southeast University, Nanjing 210096, PR China

[‡]Jiangsu Cancer Hospital, The Cancer Hospital of Nanjing Medical University, Nanjing 210009, PR China

[§]Collaborative Innovation Center of Suzhou Nano-Science and Technology, Suzhou Key Laboratory of Biomaterials and Technologies, Suzhou 215123, PR China

Supporting Information

ABSTRACT: Interventional embolization is a popular minimally invasive vascular therapeutic technique and has been widely applied for hepatocellular carcinoma (HCC) therapy. However, harmful effects caused by transcatheter arterial chemoembolization (TACE) and radioembolization, such as the toxicity of chemotherapy or excessive radiation damage, are serious disadvantages and significantly reduce the therapeutic efficacy. Here, a synergistic therapeutic strategy combined transcatheter arterial embolization and magnetic ablation (TAEMA) by using poly(lactic-*co*-glycolic acid) (PLGA)-magnetic microspheres (MMs) has been successfully applied to orthotopic VX_2 liver tumors of rabbits. These MMs fabricated by novel rotating membrane emulsification system with well-controlled sizes (100−1000 μm) exhibited extremely low hemolysis ratio and excellent biocompatibility with HepG2 cells and L02 cells. Moreover, experimental results demonstrated that, while exposed to alternating magnetic field (AMF) after TAE, the tumor edge could be heated up by more than 15 °C both in vivo and in vitro, whereas only a negligible increase of temperature was observed in the normal hepatic parenchyma (NHP) nearby. Sufficient temperature increase induces apoptosis of tumor cells. This can further inhibit the tumor angiogenesis and results in necrosis compared to the rabbits only treated with TAE. In stark contrast, tumors rapidly grow and subtotal metastasis occurs in the lungs or kidneys, causing severe complications for rabbits only irradiated under AMF. Importantly, the results from the biochemical examination and the gene expression of relative HCC markers further confirmed that the treatment protocol using PLGA-MMs could achieve good biosafety and excellent therapeutic efficacy, which are promising for liver cancer therapy.

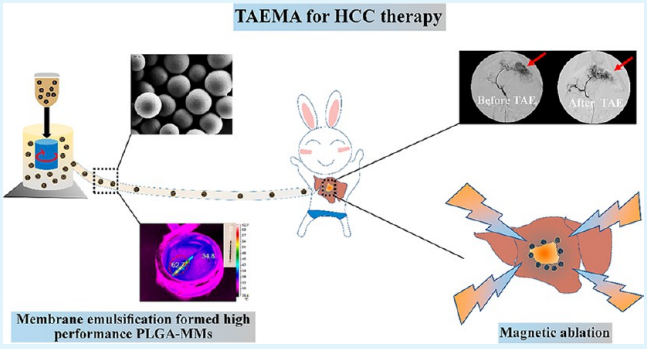

KEYWORDS: *hepatocellular carcinoma, transcatheter arterial embolization, PLGA-magnetic microsphere, membrane emulsification, magnetic ablation*

1. INTRODUCTION

Liver cancer has been typically considered as one of the deadliest and most common tumors worldwide.[1−3] In particular, treating patients with hepatocellular carcinoma (HCC) is complicated and difficult because the liver with highly vascularized and accessible capillaries can act as an ideal shelter for tumor cells.[4,5] Although the surgical resection remains the gold standard, HCC is still inoperable in many cases due to the usually late diagnosis, and due to the high recurrence rate.[6,7] Hence, developing strategies for increasing the effectiveness of the treatment remain a great challenge.

In the past few years various forms of treatments have been developed, including chemotherapy, radiotherapy, physical and chemical ablation or other local approaches.[8,9] Among these, the transcatheter arterial embolization (TAE) as a noninvasive vascular interventional treatment has a high reputation. Via the injection of the embolic agents through a catheter, the tumor feeding arteries can be effectively occluded, and consequently, the nutrition and oxygen supply can be cut off.[10−12]

Received: September 21, 2017
Accepted: November 8, 2017
Published: November 8, 2017

DOI: 10.1021/acsami.7b14330
ACS Appl. Mater. Interfaces 2017, 9, 43478−43489

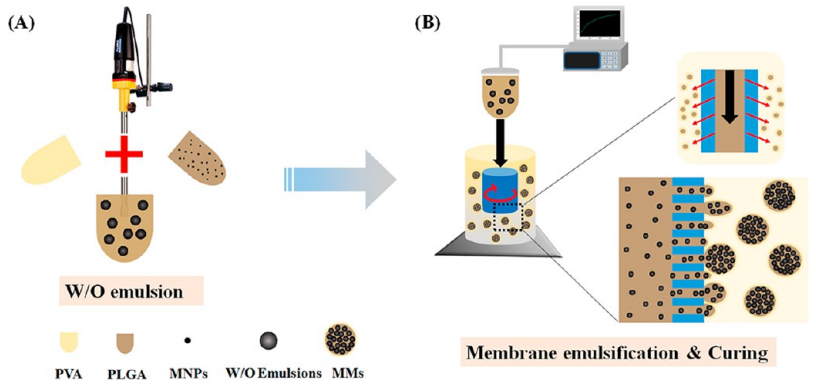

Figure 1. Schematic diagram of PLGA-MMs synthesized via rotating membrane emulsification: (A) water-and-oil emulsion process and (B) membrane emulsification process.

Clinically available embolic agents cover liquids, hydrogel and particles, etc. However, the majority so far are permanent, polydispersed, and irregularly shaped.[13] Therefore, the embolic agents mentioned above would suffer high risks regarding post-embolization syndromes and are unable to precisely control the level of embolization.[14,15] Thus, the biodegradable, regularly shaped and uniform sized microspheres should be preferred.[16] Kirchhoff and co-workers used the degradable starch microspheres (Spherex, Pharmacia, Erlangen, Germany) for the TACE procedure.[17] While co-injecting Spherex with anticancer drugs (cisplatin and doxorubicin) for occluding the target artery, the drugs could retention in a certain of time until the microspheres degraded by serum α-amylases. The clinical advantage was associated with limited tumor size and hypervascularization, which should be seen as suitable palliative measure for patients who do not tolerate long acting embolic agents. Similarly, Golzarian et.al[18] successfully prepared chitosan and carboxymethyl cellulose (CMC)-loaded doxorubicin microspheres. These biodegradable microspheres with tunable drug release profile could minimize the side effects of the chemotherapy while significantly enhancing the antitumor ability compared with other similar agents. Moreover, the experimental animal studies indicated that these biodegradable microspheres are highly promising for TACE applications. Although these widely applied therapy methods show reasonable efficacy and can reduce symptoms to some extent, they still have only limited success in HCC therapy as well as the metastasis and recurrence rates.[19]

In contrast to TACE, TAE combined with magnetic hyperthermia and ablation (TAEMH and TAEMA; the temperature between 42 and 46 °C was defined as hyperthermia, while over 50 °C was called ablation) as a promising therapeutic strategy for liver cancer treatment has attracted increasing attention. It is worth mentioning that magnetic hyperthermia with designed magnetic field and frequency can directly induce the tumor cell apoptosis above 42 °C and even cause necrosis when the temperature was greater than 50 °C (ablation). Hence, many successful cases based on this principle were reported in recent studies.[20−22] Our previous study reported that modified high-performance Mn−Zn ferrite nanocrystals exhibit an enhanced functionality for magnetically induced cancer targeted hyperthermia.[23] For instance, Yu and co-workers[24] performed the treatment with arsenic trioxide (As_2O_3) and lipiodol mixture to inhibit tumor growth and greatly improve survival of the intrahepatic VX_2 tumors in their study. They found that the antitumor effects are partly due to inhibition of tumor angiogenesis that might correlate with altered VEGF expression in the tumor and plasma. Later, Yang's team investigated the effect and feasibility of TAEMH, especially to assess the influence of heat on surrounding organs in established transplanted rabbit VX_2 hepatic tumors while exposed to AMF after embolization with ferromagnetic NPs. Results have shown that tumor growth and metastasis can be controlled by magnetically heating effectively. This would be a promising clinical treatment of HCC.[25] Although the advantages of TAEMH and TAEMA are the inhibition of tumor growth and to possibility to reach high heat in tumor regions, the continuing tumor growth as well as the inevitable damage to the surrounding organs are an issue. This is due to the magnetic fluid might escape easily from the lipiodol emulsion or microsphere suspension, and even the small-size embolic agents might increase the risk of bile duct system damage in this procedure.[26] Consequently, there is an urgent need for finding an innovative product to overcome these issues.

Poly(lactic-*co*-glycolic acid) (PLGA) is well-known as artificially synthesized polymer that has been approved by the Food and Drug Administration (FDA) and the European Medicine Agency (EMA) to serve as pharmaceutic auxiliary.[27] Therefore, we used it to develop an improved TAEMA therapeutic strategy in rabbit liver VX_2 tumor models to evaluate the feasibility, safety, and anticancer effects with respect to PLGA-magnetic microspheres (MMs). The PLGA-MMs were fabricated by the novel rotating membrane emulsification, which provides not only excellent stability and uniformity but also significant biocompatibility and biodegradability. More importantly, for both embolic agents and heating agents, remarkable magnetically induced heating effects can be achieved while exposing numerable PLGA-MMs to AMF, and the enhanced effect of embolization can be achieved by changing the phase-transition temperature of PLGA during the magnetic ablation procedure. To further evaluate the TAEMA therapy, biochemical tests and gene expressions were performed. Overall, therapeutic effect in vivo revealed that TAEMA by using PLGA-MMs show several advantages as a highly synergistic anticancer system.

2. EXPERIMENTAL SECTION

2.1. PLGA-Magnetic Microspheres Preparation. The MMs with a controllable size range from 100 to 1000 μm were prepared using a rotating membrane emulsification system (Nanotech, Changsha, China). Notably, the pores with the size of 120 ± 10 μm and the mean pitch of 1500 μm, which we used in a poly

DOI: 10.1021/acsami.7b14330
ACS Appl. Mater. Interfaces 2017, 9, 43478−43489

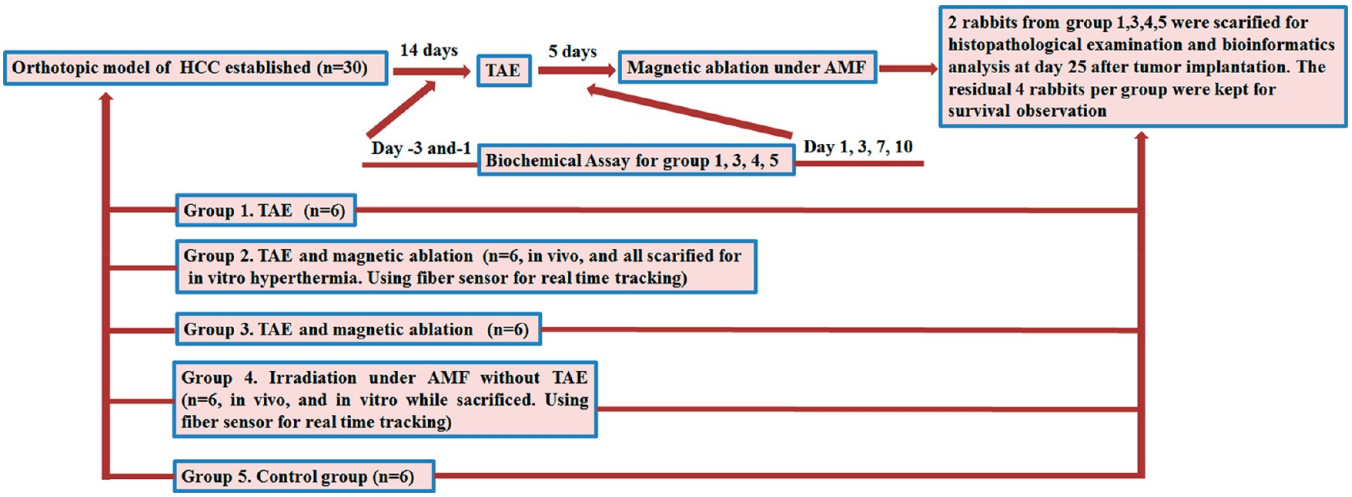

Figure 2. Flowchart of the TAE combined with the magnetic ablation (TAEMA), showing groups of rabbits and the experimental procedure.

tetrafluoroethylene (PTFE) membrane, were arranged in a cubic array, and the wall thickness of the membrane was approximately 800 μm. The preparation process was similar to that of a previously published article.[28] As schematically shown in Figure 1, first, 1 mL of 1% (w/w) PVA (Sigma-Aldrich, MO) with moderate Span-80 was added to 15 mL 5% (w/v) PLGA-dichloromethane (Daigang Biomaterial Inc., China). Afterward, 100 mg of microwave-assisted thermal decomposition approach formed Fe_3O_4 NPs[29] 20 nm in size (Monowave 300, Anton Paar, Austria) were added under intensive stirring for 5 min to form a water-and-oil emulsion (the TEM image, XRD diffraction, and hysteresis loop of as-synthesized Fe_3O_4 NPs can be found in Figure S1). Subsequently, the suspension was placed in injector, and the suitable injection speed was changed from 0.1 to 10 mL/min. Under the force generated by membrane tube rotation (with tunable speed between 200 and 800 rpm/min), the water-and-oil emulsion permeated through the porous wall into the continuous 2% (w/v) PVA phase to form uniform droplets. Afterward, the curing process was carried out by stirring the droplets at room temperature until the dichloromethane volatile completely. Finally, the obtained MMs were washed with ethanol and ultrapure water, respectively.

2.2. Characterization of PLGA-MMs. The microparticle structure and the localization as well as the structure of the embedded Fe_3O_4 NPs in PLGA-MMs was analyzed by transmission electron microscopy (TEM) and high-resolution TEM (HRTEM) using a Tokyo JEOL JEM-2100. Powder X-ray diffraction (XRD) spectra was recorded on a Bruker X-ray diffractometer (D8-Discover) operated at 40 mA and 40 kV. Meanwhile, the morphology of the as-prepared MMs was analyzed using a field-emission scanning electron microscope (SEM, Zeiss Ultra Plus, Germany) coupled with energy-dispersive spectroscopy (EDS). The infrared spectra of the Fe_3O_4 NPs and MMs was recorded with a Nicolet iS-50 Fourier transform infrared (FTIR) spectrophotometer (Thermo Fisher Scientific). The magnetism of as-synthesized Fe_3O_4 NPs and MMs were measured by a vibrating sample magnetometer (VSM, Lakeshore 7407). Iron concentrations of the MMs were evaluated using the classical 1,10-phenanthroline (phen) colorimetric method on UV−vis spectrophotometry (Shimadzu UV-3600, Japan).[30] Additionally, the total Fe_3O_4 NPs content of the MMs was obtained by thermogravimetric analysis (TGA, NETZSCH STA449 F3) employing temperatures from ambient to 800 °C with a suitable heating rate of 10 °C/min under a flow of N_2. Meanwhile, the glass transition temperatures (T_g) of the MMs was measured on a differential scanning calorimeter (DSC, PerkinElmer DSC8000) from 10 to 200 °C with same heating rate under a N_2 flow. The dichloromethane residual volume in MMs was determined by gas chromatography employing a microelectron capture detector (Agilent 7890B).

2.3. In Vitro Heat-Induction Measurements. The heating experiments of PLGA-MMs in vitro was carried out using a moderate radio frequency of a magnetic heating system (Shuangping SPG-06-II, China). The samples were dispersed in an aqueous solution with a concentration of 30 mg/mL and were placed inside a copper coil under an AMF. The temperature was measured with an FOT fiber optic sensor (FISO, Canada). Additionally, the quantitative evaluation of magnetocaloric experiment based on countable MMs was also performed under identical conditions, using thermal infrared imager (Fluke, Ti-32) for recording (1, 6, 12, and 25 MMs with sizes of 300−400 μm and 500−600 μm were capsuled into the capillary tube, respectively). Of particular importance is the specific absorption rate (SAR) for quantifying the heating efficiency of the magnetic materials when an AMF magnetic field is applied (390 kHz, 12 A). The SAR value can be calculated by the formula $SAR = C \times (dT/dt) \times (m_s/m_m)$, where C is the specific heat of the species in solution, dT/dt stands for the initial slope of the T/t curve, m_s is the weight of the whole suspension, and m_m indicates the total mass of magnetic material in suspension.[31]

2.4. Cell Culture and Cytotoxicity. HepG2 cells and HL7702 cells were originally obtained from the KeyGen Biology Technology Company (China). Cells were usually cultured under suitable conditions, grown at 37 °C in a humidified incubator with 5% (v/v) CO_2 in RPMI 1640 medium (KeyGen Biology, China), supplemented with 10% (v/v) fetal bovine serum (FBS, Sijiqing, Hangzhou, China), antibiotics (100 U/mL streptomycin and 100 U/mL penicillin). A 3-(4,5-dimethylthiazol-2-yl)-2,5-diphenyltetrazolium bromide (MTT) assay was used to evaluate the cytotoxicity of MMs. After washing with phosphate-buffered saline and UV disinfection, various concentrations of MMs (i.e., 10, 30, and 50 mg/mL, n = 4 per group) were added for co-incubated with cells at 37 °C for 12, 24, 48, and 72 h, respectively. Following this incubation, the cells were mixed with MTT (0.5 mg/mL) for 4 h, based on the standard operation. Subsequently, the absorbance at 490 nm was detected using a microplate reader (BIO-RAD680).

2.5. In Vitro Magnetic Ablation Experiments and Apoptosis Assay. HepG2 cells were either co-incubated with aseptic MMs (10 mg/mL) in a 30 mm culture dish or self- incubated and then placed inside a copper coil under AMF (390 kHz, 12 A) for 30 min. Thermal infrared imager (Fluke, Ti-32) was used for real-time tracking. Typically, the cells that were treated with MMs in ambient temperature were used as the control. The Annexin V-FITC−propidium iodide (PI) assays were carried out to evaluate apoptosis using flow cytometry (FCM). According to the manufacturer's protocol, 1×10^5 cells were treated with apoptosis assay kit (KeyGEN) for 15 min at room temperature avoiding light. Afterward FCM (FACS Calibur, BD) was used to analyze the apoptotic and necrotic status.

2.6. Hemolysis Assay. Fresh rabbit blood was collected (obtained from Model Animal Research Center of Southeast University) and preserved in a tube (BD Vacutainer) . The serum was removed from

DOI: 10.1021/acsami.7b14330
ACS Appl. Mater. Interfaces 2017, 9, 43478−43489

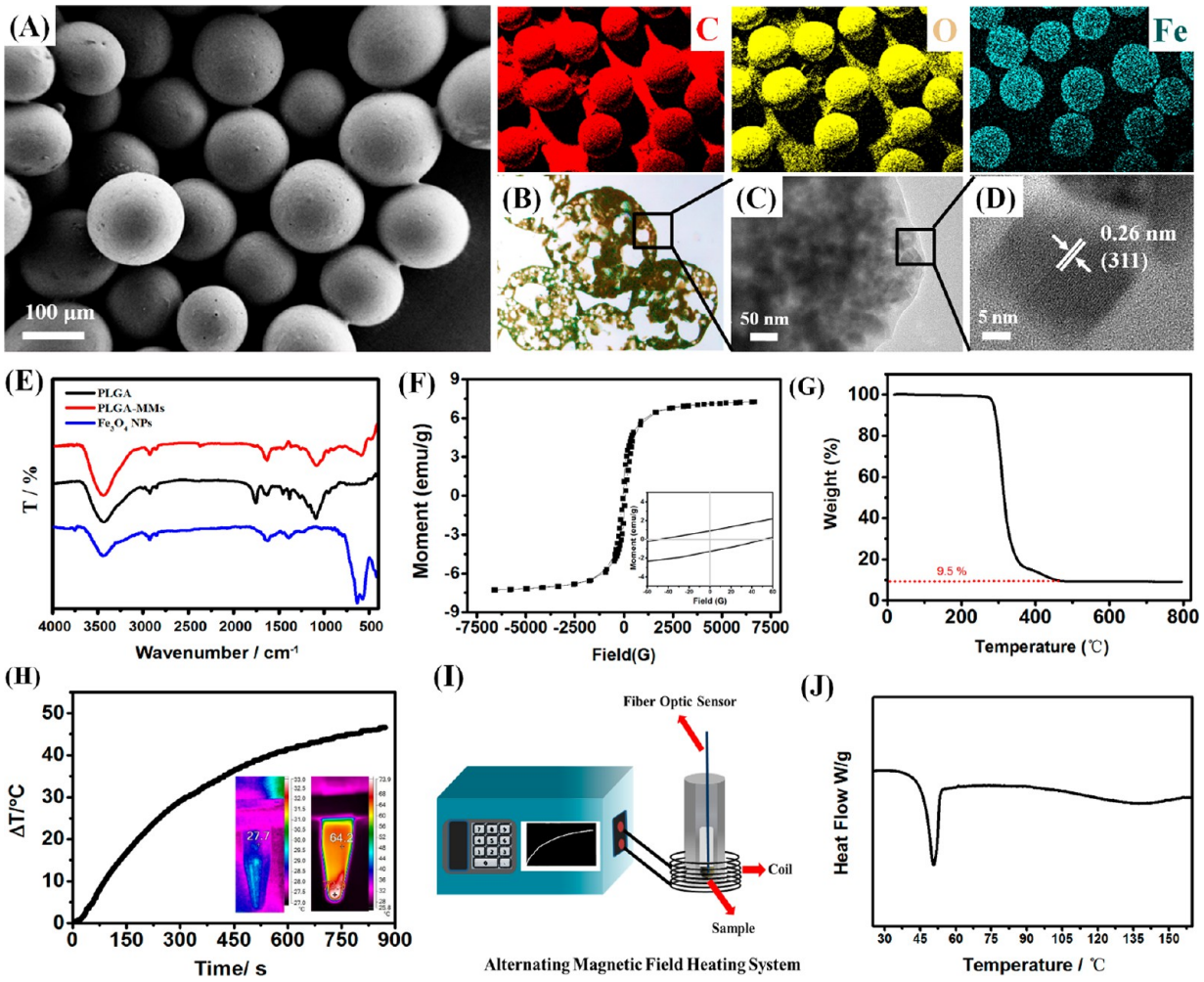

Figure 3. (A) SEM images and related element mappings of PLGA-MMs; (B) the cross-section of MMs captured by microscope (Prussian blue stain); (C) TEM and (D) HRTEM image of the embedded Fe_3O_4 NPs in MMs; (E) corresponding FTIR spectra; (F) field-dependent hysteresis loop of MMs at room temperature; (G) TGA curve of MMs; (H) time-dependent temperature curves of MMs (insets are near-infrared images before and after heating); (I) schematic drawing of magnetically induced heating; and (J) DSC curve of MMs.

rabbit blood by centrifugation for 15 min at 1800 rpm/min. The supernatant phase was removed and the residual blood cells at the bottom were washed fully with sterilized saline (0.9%, w/v). The blood cells were diluted (1:10) with 0.9% (w/v) saline to form 2% (v/v) suspension after washing. To the suspension were added: (A) 50 mg/mL MMs solution, (B) 30 mg/mL MMs solution, (C) 10 mg/mL MMs solution, (D) 5 mg/mL MMs solution, equal volume of (E)sterilized saline and (F)distilled water. The mixture was used as a negative and positive control, respectively. The mixtures were stirred at room temperature for 2 h. Finally, they were centrifuged, and the OD values of the supernatant clear solutions were measured at 540 nm, using a Shimadzu UV-3600 UV−vis absorption spectrophotometer. The percentage of hemolysis rate (HR) for MMs samples in various concentration was calculated as $HR = (OD_{MMs} - OD_{negative})/(OD_{positive} - OD_{negative})$.[32]

2.7. Biodegradation Assay in Vitro. The biodegradation assay was carried out by simulating the in vivo environment, while the PLGA-MMs were co-incubated in culture medium, which was as similar to the cell culture mentioned above, except the fact that antibiotics were abandoned. Samples were selected randomly at day 1, 5, 15, 30, 45, and 60; washed fully with ultrapure water; and then measured by SEM.

2.8. Animal Models and Experimental Protocol. Thirty male New Zealand white rabbits (3−3.5 kg in weight, $n = 6$ per group) were purchased from the Model Animal Research Center of Southeast University, and all animal experimental procedures were in accordance with the guidelines of the Institutional Animal Care and Use Committee of Southeast University (license no. SYXK-2016-0013). Figure 2 shows the flowchart of experiment protocol. The orthotopic models of liver tumors were established by using VX_2 carcinoma as previously reports.[24,33] The rabbits from group 1, 2, and 3 received the TAE 2 weeks after tumor implantation. Magnetic ablation was induced on day 5 after TAE for group 2 and 3. Group 4 received the same irradiation procedure under AMF but without TAE. Group 5 was used as control. Finally, two rabbits were randomly selected from groups 1, 3, 4, and 5 and were sacrificed on day 25 after implantation for histopathological examination and bioinformatics analysis, whereas the other four rabbits in each group were kept for survival observation.

2.9. Treatment Procedure. TAE was carried out on day 14 after tumor implantation. First, rabbit was anesthetized by 2% (w/v) sodium pentobarbital (1 mL/kg intravenous infusion, Sigma-Aldrich, MO), and a 4F vascular sheath was then placed into the femoral artery (Terumo, Tokyo, Japan). Selective catheterization to the hepatic artery feeding carcinoma was achieved by utilizing a 2.7 F microcatheter (Terumo, Tokyo, Japan) under DSA, which can guarantee tumor targeted embolization and spared arterial flow through the hepatic artery into the liver. Subsequently, a mixture containing 30 mg MMs (100−150 μm) and moderate contrast agent (iohexol, Yangzijiang Pharmaceutical Co., China) was then carefully injected into the tumor-feeding artery via microcatheter. After that, irradiation protocol was applied on day 5 after TAE for group 2 and 3 using a moderate radio frequency of magnetic heating system (Shuangping SPG-10-III,

DOI: 10.1021/acsami.7b14330
ACS Appl. Mater. Interfaces 2017, 9, 43478−43489

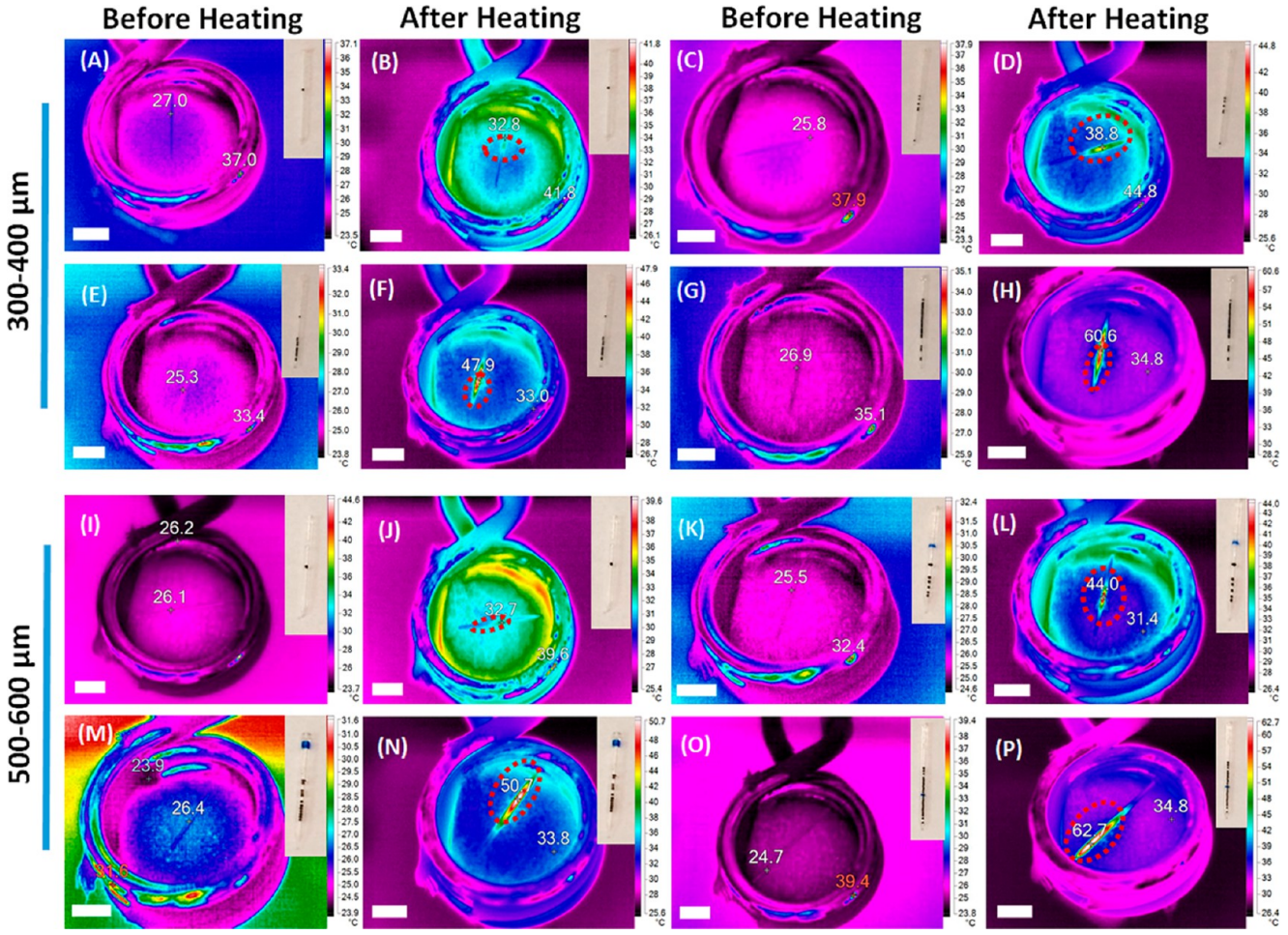

Figure 4. Quantitative evaluation of magnetic-induced heating performance based on 1, 6, 12, and 25 PLGA-MMs of 300−400 μm in size (panels A−H) and 500−600 μm (panels I−P), respectively. Thermal infrared imager was used for real-time tracking, and the insets are different numbers of MMs that capsuled into the capillary tube. Scale bar: 1 cm.

China), as well as for group 4 (without TAE). All rabbits received the anesthesia procedure as described above and were then treated with AMF (500 kHz, 16A) for a period of 30 min. To verify the efficiency of the magnetic ablation induced by high-performance MMs, the rabbits in group 2 were sacrificed after in vivo ablation. The liver was removed immediately for in vitro ablation under identical conditions. The similar in vitro irradiation procedure also applied for group 4 while rabbits died.

2.10. Biochemical Assay. Fresh serum (2.0 mL/sample) of group 1, 3, 4, and 5 was collected for biochemical examination on day 3 and day 1 before the TAE and also on day 1, 3, 7, 10 after the treatment. The alanine transaminase (ALT), aspartate aminotransferase (AST), and blood urea nitrogen (BUN) as well as creatinine (Cr), and total bilirubin (TBil) levels were measured using a biochemical auto analyzer (Beckman AU5800).

2.11. Histopathological Analysis. The rabbits were sacrificed by intravenous injection of overdose of sodium pentobarbital for histopathological evaluation. The liver was removed and stabilized with 4% (v/v) buffered formalin for paraffin section preparation. All paraffin-embedded samples were stained with hematoxylin and eosin (H&E), and the histopathological pictures were finally taken using a microscopy imaging system (Nikon ECLIPSE E200, Japan)

2.12. RNA Isolation and Quantitative Polymerase Chain Reaction. Total RNA was isolated from fresh hepatic tissue of each group using Trizol Reagent (Invitrogen Life Technologies) according to the manufacturer's protocols and then converted into cDNA by using Revert Aid First Strand cDNA Synthesis Kit (Thermo Scientific). Afterward, real-time quantitative polymerase chain reaction (Q-PCR) was performed using Fast Start Universal SYBR Green Master (Roche, Switzerland). The information on gene-specific primers is shown in Table S1, and the relative quantification of gene expression was evaluated using the $2^{-\Delta\Delta Ct}$ method.[34] Each sample was tested in triplicate and threshold values were determined, average values and mean standard deviation were also calculated, and the mRNA levels were normalized to the GAPDH (housekeeping gene) in same sample.

3. RESULTS AND DISCUSSION

3.1. Characterization of PLGA-MMs. The SEM images of as-prepared PLGA-MMs, which consist of microwave-formed Fe_3O_4 NPs, were shown in Figure 3A. These MMs have smooth surfaces and show relatively uniform size distribution from 100 to 150 μm. One can be clearly see from the element mappings that the elements Fe, O, and C were distributed uniformly on the surface of each sphere-like structure. In particular, the sponge-like structure was found inside the spheres while capturing the cross-section of MMs by microscope (Figure 3B, Prussian blue stain). Furthermore, the localization, as well as structure of embedded Fe_3O_4 NPs were also confirmed by TEM and HRTEM, respectively (Figure 3C,D).

As shown in Figure 3E, the analyses of PLGA-MMs examined using FTIR revealed the presence of characteristic absorbance peaks in the regions of 1082, 1745, 2924, and 3480 cm^{-1}, which can be assigned to C−O−C, C═O, C−H, and

DOI: 10.1021/acsami.7b14330
ACS Appl. Mater. Interfaces 2017, 9, 43478−43489

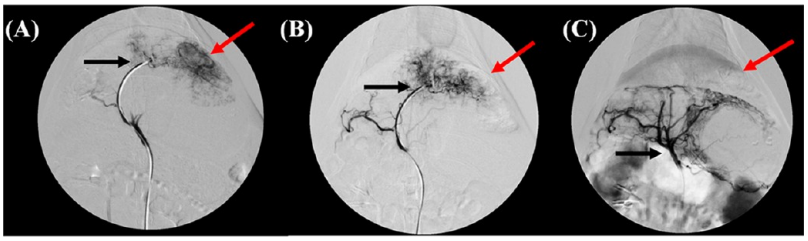

Figure 5. Angiography of the hepatic artery. (A) The stain of a hyper-vascular tumor (red arrow) in the left lobe of liver before embolization. (B) The feeding arteries of the tumor were successfully occluded by PLGA-MMs after embolization. (C) DSA image of the completed hepatic angiography after TAE (black arrow indicates the 2.7F microcatheter in the hepatic artery).

−OH vibration modes for PLGA.[35] Fe_3O_4 NP induce peaks at 570 and 3450 cm^{-1} can be assigned to the Fe−O and −OH stretching vibration absorption. The bending vibration of −OH was confirmed by the peak at 1624 cm^{-1}.[36] In addition, the magnetic performance of MMs is of great importance for their biomedical applications. The M_s of MMs measured by VSM at ambient temperature showed an excellent magnetization value of 7.2 emu/g, and slight remaining magnetization was observed in hysteresis loop for MMs (Figure 3F). Based on the result in Figure 3G, the completed thermal decomposition of the PLGA resulted in a weight loss of 90.5% at 500 °C, and the residue turned out to be iron oxides. Moreover, the magnetically induced heating measurement in alternating magnetic field (AMF, 390 kHz, 12 A) shows an SAR of 415 w/g of the as-prepared MMs with a concentration of 30 mg/mL in aqueous solution (the specific heat capacity of an aqueous solution is 4.2 $kJ{\cdot}kg^{-1}{\cdot}K^{-1}$), (Figure 3H,I). Due to the excellent magnetic heat induction effect of the MMs, the temperature is much higher than the glass transition temperature (T_g) of PLGA (50 °C, Figure 3J), which leads to a significant increase of the molecular motion that caused by phase transition from the glassy state to the rubbery state. The gas chromatography with ECD pattern was used to measure the residual volume of dichloromethane in PLGA-MMs.[37] The result 0.034% is far below the International Conference on Harmonization (ICH) standard for drug registration and technique requirements of 6 mg/day or 600 ppm.[38]

3.2. In Vitro Performance Evaluation of PLGA-MMs. As presented in Figure 4, the quantitative evaluation of magnetic-induced heating performance based on countable MMs (i.e., 1, 6, 12, and 25) with sizes of 300−400 μm and 500−600 μm indicated that temperature rise along with the quantity of MMs increase. In particular, the temperature of 6 MMs, which capsuled into the capillary, were detected to be ca. 39 °C (300−400 μm in size) and 44 °C (500−600 μm), respectively, while encapsulated 25 MMs then possess the maximum of ca. 60 °C (with size of 300−400 μm) and 63 °C (500−600 μm), respectively. The outstanding heating efficiency by exposing numerable MMs to AMF was attributed to the microwave formed Fe_3O_4 NPs, so that the M_s value and SAR value of obtained PLGA-MMs were higher than the reported polymer MMs with similar size or with the same mass of iron.[39,40]

To evaluate the cytotoxicity and biocompatibility of PLGA-MMs, we performed a cell viability assay. HepG2 cells and HL7702 cells were treated with various concentrations of MMs for 12, 24, 48, and 72 h respectively, and then we employed MTT incubation to determine cell viability. The results showed that the cells possess a viability of more than 95% at all tested dosage and all exposure time, even after an exposure for 72 h with concentration 50 mg/mL (Figure S2). We also conducted Annexin V/PI apoptosis assay of MMs using HepG2 cells. Results in Figure S3 showed that the ratio of living cells decreased sharply while applying AMF for 30 min with MMs, which indicates the magnetothermal effect by MMs is responsible for both apoptosis and subsequent necrosis.[41]

As can be seen from Figure S4, the degree of hemolysis induced by MMs show no significant difference to the negative control (saline). Apparently, MMs show extremely low hemolysis rate, even applying the maximum dosage of 50 mg (3.3%), which is considered as a critical safe hemolytic ratio (less than 5%) according to ASTM F756 and ISO/TR 7406.[42] Because the duration of embolization is a critical issue, the biodegradation of MMs was traced under simulated in vivo condition and used SEM to record at day 1, 5, 15, 30, 45, and 60, respectively. As shown in Figure S5, the surface of MMs became rough on day 15, the exfoliation occurred at day 30. Although slightly cracks could be observed at day 60, the MMs remain in optimal shape, which demonstrated that it takes very long until the as-prepared PLGA-MMs are degraded. It should note that the degradation behavior of PLGA is closely related to the molecular weight, as well as the chain ratio of LA and GA. All of the in vitro results suggest that the PLGA-MMs can be considerable for HCC therapy with TAEMA.

3.3. TAEMA Treatment Process Using PLGA-MMs. The PLGA-MMs mediated therapeutic protocol combining TAE and magnetic ablation for HCC treatment as shown in Figure 2. Usually a mixture containing iodized oil and magnetic fluid is used as reported in the previous investigations.[24,43−45] However, the dose limitation and detention time of iodized oil, as well as the unavoidable problem of leaking magnetic fluid, still remains a great challenge for ensuring the curative effect. Our results of the in vitro evaluation using the PLGA MMs show significant advantages of TAEMA compared with current methodologies. These advantages can be ascribed to the use of the MMs, which show a synergistic antitumor effect because of two important properties: their effective embolization and their outstanding magnetothermal performance.

The TAE process was performed using a digital subtraction angiography system (DSA, Philips, BV Pulsera) according to clinical regulations. The angiography showed that the tumor was surrounded by rich blood capillaries, especially at the edge (Figure 5A). Notably, blood vessels of its neighboring normal hepatic parenchyma (NHP) were swollen after embolization, which indicates that MMs were deposited in the area of the lesion to a significant extend and consequently blocked the feeding routes (Figure 5B,C). In comparison to hepatic angiography, the corresponding computed tomography (CT, GE, HiSpeed NX/I) showed inconspicuous gray variation before TAE because the contrast agent was metabolized too fast to be traced (Figure S6A). However, an enhanced signal in the

DOI: 10.1021/acsami.7b14330
ACS Appl. Mater. Interfaces 2017, 9, 43478−43489

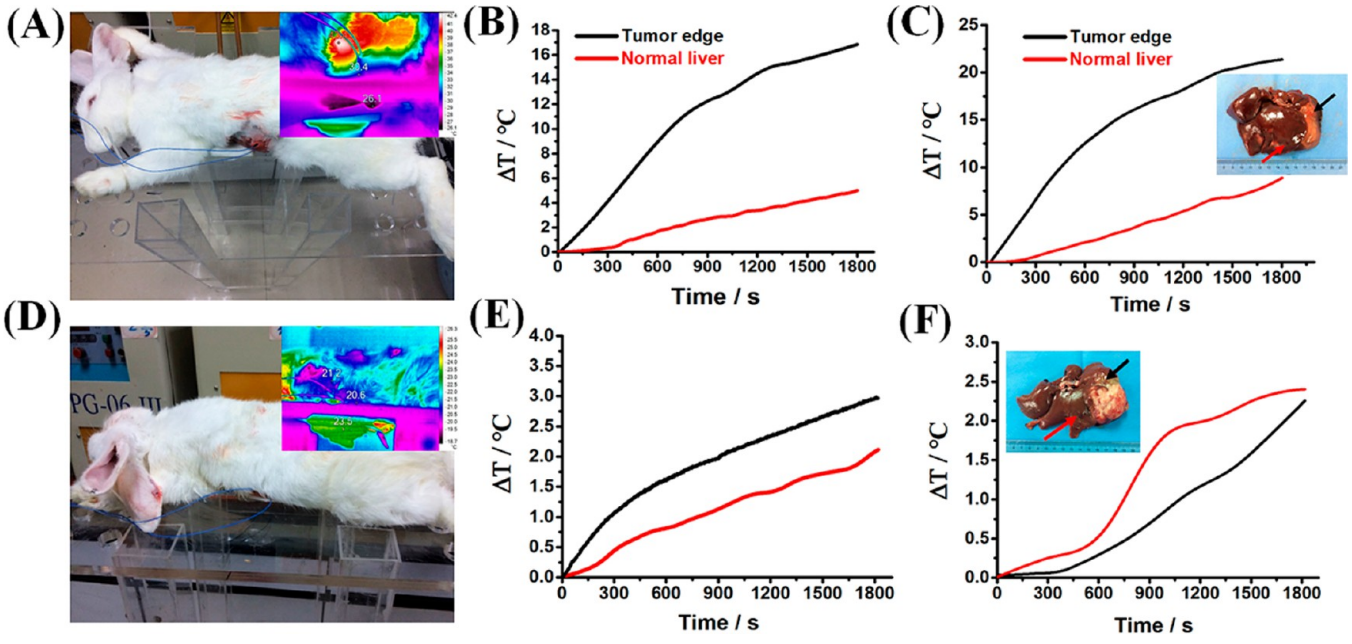

Figure 6. Real-time temperature monitoring for magnetic ablation in group 2. (A) A photograph of a rabbit of group 2 in AMF (inset is near-infrared image); (B) in vivo and (C) in vitro time-dependent temperature curves of liver tissue; (D−F) the in vivo and in vitro time-dependent temperature curves of liver during irradiation with AMF for a group 4 rabbit (treated under identical conditions). Black and red arrows indicate the location where optical fiber inserted in tumor edge or NHP.

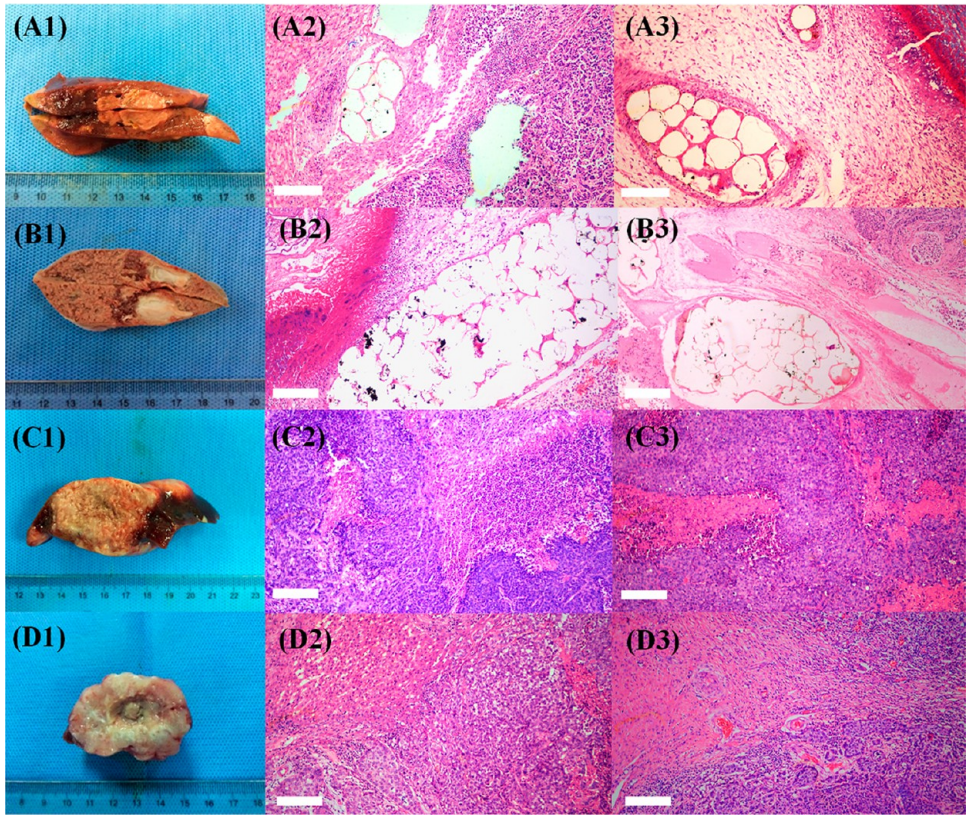

Figure 7. Histopathological images of liver in each group (H&E stain). (A1) Pathological specimen of TAE in group 1. (A2, A3) Pathological sections of TAE in group 1. (B1) Pathological specimen of TAEMA in group 3. (B2, B3) Pathological sections of TAEMA in group 3. (C1) Pathological specimen of group 4 (only irradiation under AMF). (C2, C3) Pathological sections of group 4. (D1) Pathological specimen of control group. (D2 and D3) Pathological sections of control group. All of the images of pathological sections were taken at 100× magnification. Scale bar: 200 μm.

tumor region was obtained after 2 h of TAE (Figure S6B), revealed that the contrast agent within the mixture of MMs was trapped in peripheral vascular. Furthermore, the artifact of magnetic resonance imaging (1.5T MR scanner, Philips, MR

DOI: 10.1021/acsami.7b14330
ACS Appl. Mater. Interfaces 2017, 9, 43478−43489

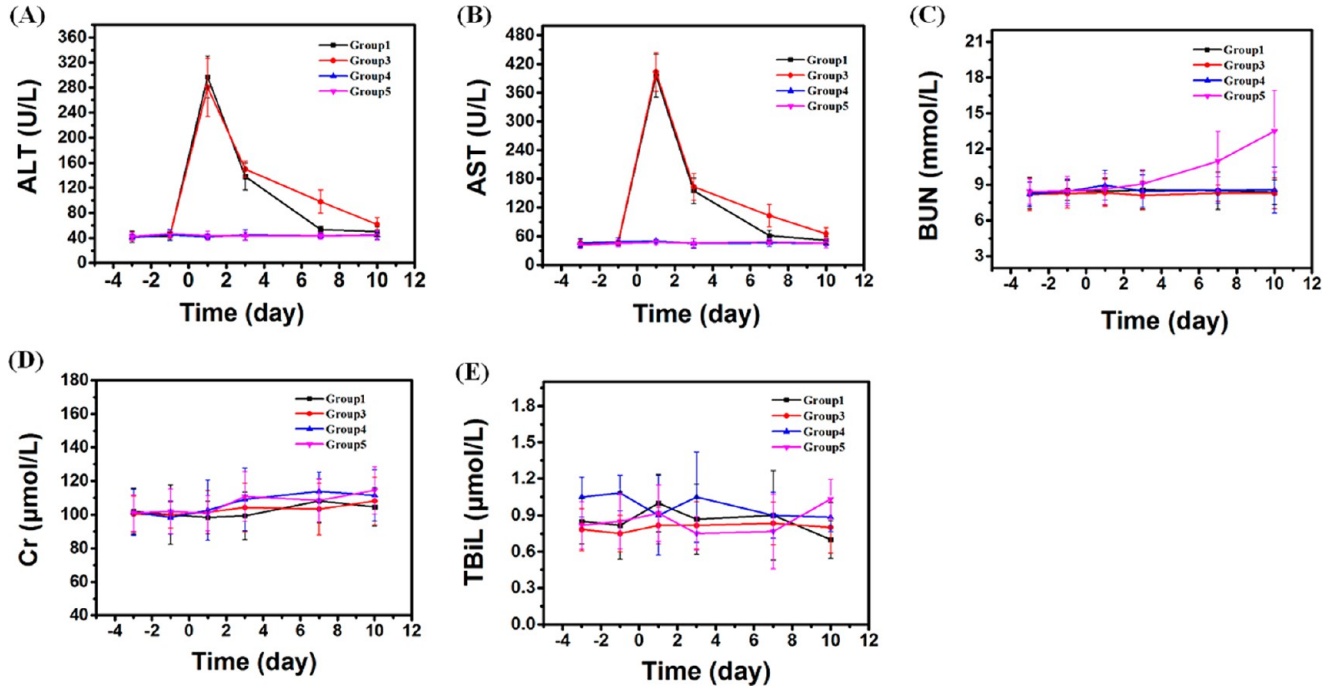

Figure 8. Biochemical tests of (A) ALT levels, (B) AST levels, (C) BUN values, (D) plasma Cr values, and (E) plasma TBil levels.

Systems Achieva), which further indicated that the MMs are still trapped around the tumor at day 5 after TAE (Figure S6C).

To demonstrate the MMs heating ability to tumors, rabbits in group 2 and 3 after TAE on day 5, and also the rabbits of group 4 after tumor implantation were fixed in a bowl-shaped coil to performed the irradiation under AMF. For real-time temperature tracking, the rabbits' abdomen in group 2 and 4 were opened and two fiber sensors (FOT series fiber optic sensor, FISO, Canada) were inserted into their liver. Note that one fiber sensor was located in the tumor edge, while the other was placed in the surrounding NHP, and all the data of temperature recording was summarized in Table S2. After exposure to the AMF, the temperature of the tumor edge in group 2 started to increase and was still rising. Finally, the ΔT was more than 15 °C in 30 min, while the NHP of the liver just increased its temperature by less than 5 °C without damaging neighboring healthy tissue[46] (Figure 6A,B). In contrast, the temperature measurement for group 4 revealed only poor heating. This low heat increase can be attributed to the convective heat transfer of copper coil (Figure 6D,E). We also performed the in vitro ablation procedure for rabbits in group 2, which were sacrificed after in vivo thermotherapy, whereas the rabbits in group 4 received the AMF irradiation while they died. As expected, the same heating performance was observed (Figure 6C,F).

3.4. Evaluation of the Therapeutic Effect of TAEMA. It was evident that the tumor-inhibiting effect after TAE was due to the super selective embolization of MMs cutting off the nutrition supply, which is necessary for tumor survival. This results in the devascularization and progressive shrinkage of the tumor[47] (Figure 7A1, group 1). TAEMA is a complementary treatment that consists of selective arterial embolization and AMF exposure to generate efficiently heat over 50 °C. Because the blood vessel in tumor is chaotic and tortuous that caused the blood flow inside unlike others. Thereby, the heat conduction and cooling mechanisms of tumor ablation might lead to the highly vascularized tumor edge acting as a container to accumulate heat energy and then transfer to the tumor core or normal tissue in contrast to the other part of liver.[48] Continuous temperature above 50 °C can cause cancer cells more sensitive and render massive necrosis in a certain extent, which leads to a thick fibrocollagenous capsule around the tumor eventually,[49] Figure 7B1 (group 3). In contrast, the process of artery occlusion to prevent nutrient supply, combined with magnetic ablation for acute necrotizing of the tumor has not been performed for group 4 (irradiation under AMF only) and group 5 (control), so that intrahepatic metastasis occurred[50] (Figure 7C1,D1). Evidence also can be seen that based on the pathologic specimens of Figure S7. The necrosis area that caused by TAE and TAEMA was found in the left lobe of liver for group 1 and 3 (the first and the second row). Especially, the sign of heating is noticeable on the surface around the tumor site (group 3), which indicated that the TAEMA has good therapeutic effect. However, the size of tumor in group 4 and 5 was found much bigger than group 1 and 3, and the biological features of infiltrative growth was also observed. In particular, according to the cross-section of tumor in group 4 and 5, it contained focally rather small necrosis in the center and additionally small cavernous vessels, such a feature was strongly correlated to tumor malignancy. Consequently, a number of tumor metastasis and severe complication were seen elsewhere in the pathologic specimens of lungs and kidneys for group 4 and 5, respectively (Figure S7, third and fourth row).

In addition, histological examination of livers from each group was performed to further evaluate the antitumor effect of TAEMA. The slices of group 1 (Figure 7A2,A3) clearly showed that the majority of MMs were blocking and agglomerating in the small arterial vessel around the tumor. Meanwhile, the infarction, which was associated with tumor cell degeneration and necrosis, was also observed in the tumor tissue. The main pathologic changes after TAEMA (group 3, Figure 7B2,B3) presented larger infarctions (areas of coagulative necrosis) close to the tumor edge compared to TAE due to the high

DOI: 10.1021/acsami.7b14330
ACS Appl. Mater. Interfaces 2017, 9, 43478−43489

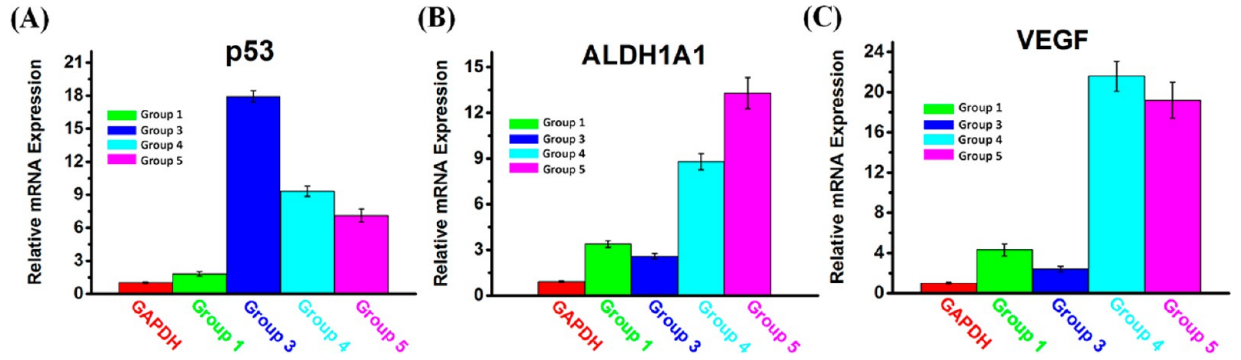

Figure 9. Analysis of mRNA expression by Q-PCR: (A) p53, (B) ALDH1A1, and (C) VEGF, respectively; GAPDH was used as a house-keeping gene.

temperature that would make the vacuolization of cytoplasm worse and consequently result in extensive necrosis to the tumor region. However, the observation of pathologic changes for both TAE and TAEMA were in sharp contrast to the group only treated with irradiation (Group 4, Figure 7C2,C3) and control group (Group 5, Figure 7D2,D3), while the phenomenon of cancer cell proliferation can be found in abundance in the tumor tissue. More importantly, the phase transition of PLGA induced by sufficient temperature elevation plays crucial role for therapy. Because the high temperature above the T_g (50 °C) would cause adhesion behavior by melting of the surface of PLGA microspheres. The hypothesis was confirmed via pathological sections with Prussian blue stain of TAE (group 1, Figure S8A1−A3) and TAEMA (group3, Figure S8B1−B3), respectively. Therefore, the advantage of PLGA-MMs should be highly promising to achieve the enhance effect of embolization through the aggregation on long-term and the adaptive deformation in tumor vessels.

As exhibited in Figure 8A,B, ALT and AST levels of group 1 and 3 increase significantly compared with the other groups on day 1 after the TAE but decrease to levels close to normal within further 10 days, indicated the TAEMA was successfully performed without affecting the liver function. It should mentioned that the ALT and AST levels of group 3 went up slightly after magnetic ablation compared with those that just received TAE at the same time (day 5 after TAE), whereas there is no indication of change for group 4 rabbits only received the irradiation. However, there is no distinct difference in the plasma Cr and TBil levels for any group (Figure 8D,E); however, the BUN level change in group 5 was in contrast to the others, and it might be due to the tumor metastasis, which would eventually affect renal function (Figure 8C).

To acquire more concrete proof that TAEMA is an effective and feasible strategy, the real-time relative-quantitative polymerase chain reaction (Q-PCR) was used to investigate the expressive changes of important genes related to the HCC, including tumor protein p53 (p53),[51] aldehyde dehydrogenase 1 family (ALDH1A1, also known as retinaldehyde dehydrogenase 1),[52] and vascular endothelial growth factor (VEGF), respectively.[53] In fact, p53 possesses sophisticated mechanisms of anticancer function and plays a role in apoptosis, genomic stability, and inhibition of angiogenesis. Meanwhile, the enzymatic activity of ALDH1A1 has been identified as one of the markers of cancer stem cells, and the high expression is associated with prognosis in a variety of solid tumors.[54] Furthermore, tumors usually secrete a series of materials that accelerate the speed of vascularization. Owing to the incomplete structure and deficient function of neovascularization, tumor cells may into the circulation by enhanced permeability and retention (EPR) effect then cause metastasis.[55] These findings provide evidence for the successful application of PLGA-MMs in HCC therapy and understand the TAEMA's antitumor mechanism on molecular level.

As shown in a previous report the mRNA expression level of related markers in HCC can be down-regulated after the therapy.[56] As shown in Figure 9A, low-level p53 expression was observed for group 1 rabbits. This is in stark contrast to the highly expressed group 4 and 5, which suggests that the growth of tumor could be effectively suppressed by TAE treatment.[57] However, the behavior in group 3 (TAEMA) was up-regulated 2−3 fold because p53 is acting as a heat-shock protein, so that thermal induced activation leads to significant increase of the expression in body.[58] According to the result in Figure 9B, the expressions of ALDH1A in group 4 and 5 were up-regulated 5−6 fold to group 1 and 3, the abnormal expression may be related to tumor occurrence, invasion, and metastasis.[59] Meanwhile, the overall response in group 3 was better compared to group 1, which also demonstrated the TAEMA achieve better therapeutic effect than TAE. High VEGF protein expression was used as a factor for tumor-growth prediction. The results presented in Figure 9C for VEGF expression were similar to the trend of p53. The value detected from group 4 and 5 rabbits was over-expressed in comparison with group 1 and 3, which means the permeability of the vessel increased. This leads to acceleration of spreading of endothelial cells and was responsible for the activation of angiogenesis in tumor growth and metastasis.[60]

Moreover, the survival curve based on Kaplan−Meier method[61] (Figure S9) exhibits a significant survival benefit for rabbits in group 1 and 3, which were treated with TAE or TAEMA (with the longest survival time of 54 day) compared with those with extensive tumor in groups 4 and 5 (survival time of less than 33 days). The MMs can induce tumor ischemia and hypoxia as well as the continuous release of heat into the lesions. Consequently, they can selectively kill tumors in a long-lasting manner. Our results further demonstrated that applied PLGA-MMs for TAEMA could provide a dramatically improved therapeutic efficacy in HCC therapy.

CONCLUSIONS

In summary, we have successfully developed a combined embolization magnetic ablation strategy for orthotopic hepatocarcinoma therapy using VX_2 orthotopic models. The rotating membrane emulsification system formed PLGA-MMs

DOI: 10.1021/acsami.7b14330
ACS Appl. Mater. Interfaces 2017, 9, 43478−43489

with ideal behavior, and the treatment protocol finally resulted in excellent synergistic therapeutic effects. We could suppress associated tumor angiogenesis and also cause necrosis of tumor cells due to comparably high magnetically induced temperatures. More importantly, the phase transformation of PLGA from the glassy state to the rubbery state that induced by magnetic heating effects could enhance MMs aggregation, and subsequently leading to longer lasting of embolization in tumor regions without severe side effects. Additionally, performed biochemical test demonstrated that the TAEMA using PLGA-MMs has a limited effect on liver and kidney function. Especially, the expression changes of HCC related makers show how TAEMA affect the outcomes from molecular level. Our results demonstrate that the TAEMA strategy using high-performance PLGA-MMs is another highly promising strategy for HCC therapy besides TACE and radioembolization. Detailed investigation of the PLGA-MMs metabolism in vivo and further experiment to evaluate the mechanism for TAEMA are underway.

■ ASSOCIATED CONTENT

Supporting Information

The Supporting Information is available free of charge on the ACS Publications website at DOI: 10.1021/acsami.7b14330.

Corresponding characterization of the Fe_3O_4 NPs, related cytotoxicity data, in vitro magnetic ablation of PLGA-MMs and corresponding apoptosis rates, the hemolysis rate of PLGA-MMs, data on in vitro degradation of PLGA-MMs, CT images and MR image of TAE and pathologic specimens, pathological sections with Prussian blue stain, and the Kaplan−Meier survival analysis of living rabbits, related primer pairs used in q-PCR, and the real-time temperature monitoring for rabbits in group 2 and group 4. (PDF)

■ AUTHOR INFORMATION

Corresponding Authors

*E-mail: 13813939190@139.com.
*E-mail: guning@seu.edu.cn.
*E-mail: zhangyu@seu.edu.cn.

ORCID

Ning Gu: 0000-0003-0047-337X

Author Contributions

‖Y.-J.L., H.Y., and G.F. contributed equally to this work. Y.-J.L. (PhD candidate) is responsible for experimental design and manuscript writing. H.Y. (M.D.) and G.D.F. (M.D.) are in charge of the TAEMA process. All authors participated in data analysis and results discussion and gave approval to the final version of the manuscript.

Notes

The authors declare no competing financial interest.

■ ACKNOWLEDGMENTS

We express our deepest condolence to all of the rabbits sacrificed for scientific research in this work and greatly appreciate Dr. Jennifer M. Kremsner (Anton Paar GmbH) to improve the English writing. We thank Mr. Quan Hu (Nanotech, Changsha) for the membrane emulsification system and technical support. Dr. Yang Gao and Dr. Lei Sun (Department of Radiology, Jiangsu Cancer Hospital) as well as Dr. Zhen Guo (Department of Image, Jiangsu Cancer Hospital) are greatly appreciated for their help in results discussion and imaging support. We also thank Dr. Feng Yan (Clinical Laboratory, Jiangsu Cancer Hospital) and Dr. Longfei Wang (Department of Pathology, Zhongda Hospital Affiliated to Southeast University) for their help in biochemical detection and pathologic analysis, respectively. This research is supported by the National Key Research and Development Program of China (no. 2017YFA0205502), the National Program on Key Basic Research Project (973 program, no. 2013CB733800), the National Natural Science Foundation of China (nos. 81571806, 81271677, and 81671820), and the National Natural Science Foundation of China for Key Project of International Cooperation (no. 61420106012). The funding from Collaborative Innovation Center of Suzhou Nano Science and Technology (grant no. SX21400213) and a Talent 333 Project in Jiangsu Province (no. BRA2015492) are also appreciated.

■ REFERENCES

(1) Dart, A. Tumorigenesis: Cancer Goes Tick Tock. *Nat. Rev. Cancer* **2016**, *16*, 409−409.
(2) Siegel, R. L.; Miller, K. D.; Jemal, A. Cancer Statistics, 2017. *Ca-Cancer J. Clin.* **2017**, *67*, 7−30.
(3) Omata, M.; Lesmana, L. A.; Tateishi, R.; Gani, R. A.; Rinaldi Lesmana, C.; Putranto, A. T.; Liaw, Y. F.; Sarin, S. K. Asian Pacific Association for the Study of the Liver Consensus Recommendations on Hepatocellular Carcinoma. *Hepatol. Int.* **2010**, *4*, 439−474.
(4) Villanueva, A.; Llovet, J. M. Liver cancer in 2013: Mutational Landscape of HCC [mdash] the End of the Beginning. *Nat. Rev. Clin. Oncol.* **2014**, *11*, 73−74.
(5) Yang, J. D.; Roberts, L. R. Hepatocellular Carcinoma: a Global View. *Nat. Rev. Gastroenterol. Hepatol.* **2010**, *7*, 448−458.
(6) Shah, S. A.; Cleary, S. P.; Wei, A. C.; Yang, I.; Taylor, B. R.; Hemming, A. W.; Langer, B.; Grant, D. R.; Greig, P. D.; Gallinger, S. Recurrence After Liver Resection for Hepatocellular Carcinoma: Risk Factors, Treatment, and Outcomes. *Surgery* **2007**, *141*, 330−339.
(7) Roayaie, S.; Jibara, G.; Tabrizian, P.; Park, J. W.; Yang, J.; Yan, L.; Chen, M.; Blanc, J. F.; Johnson, P.; Roberts, L. R.; et al. The Role of Hepatic Resection in the Treatment of Hepatocellular Cancer. *Hepatology* **2015**, *62*, 440−451.
(8) Genco, C.; Cabibbo, G.; Maida, M.; Brancatelli, G.; Galia, M.; Alessi, N.; Butera, G.; Giarratano, A.; Midiri, M.; Cammà, C.; et al. Treatment of Hepatocellular Carcinoma: Present and Future. *Expert Rev. Anticancer Ther.* **2013**, *13*, 469−479.
(9) Flores, A.; Marrero, J. A. Emerging Trends in Hepatocellular Carcinoma: Focus on Diagnosis and Therapeutics. Clinical Medicine Insights. *Oncology* **2014**, *8*, 71−76.
(10) Sato, M.; Tateishi, R.; Yasunaga, H.; Horiguchi, H.; Yoshida, H.; Matsuda, S.; Koike, K. Mortality and Morbidity of Hepatectomy, Radiofrequency Ablation, and Embolization for Hepatocellular Carcinoma: a National Survey of 54,145 Patients. *J. Gastroenterol.* **2012**, *47*, 1125−1133.
(11) Rammohan, A.; Sathyanesan, J.; Ramaswami, S.; Lakshmanan, A.; Senthil-Kumar, P.; Srinivasan, U. P.; Ramasamy, R.; Ravichandran, P. Embolization of Liver Tumors: Past, Present and Future. *World journal of radiology* **2012**, *4*, 405−412.
(12) Llovet, J. M.; Real, M. I.; Montaña, X.; Planas, R.; Coll, S.; Aponte, J.; Ayuso, C.; Sala, M.; Muchart, J.; Solà, R.; Rodés, J.; Bruix, J. Arterial Embolisation or Chemoembolisation Versus Symptomatic Treatment in Patients with Unresectable Hepatocellular Carcinoma: a Randomised Controlled Trial. *Lancet* **2002**, *359*, 1734−1739.
(13) Osuga, K.; Maeda, N.; Higashihara, H.; Hori, S.; Nakazawa, T.; Tanaka, K.; Nakamura, M.; Kishimoto, K.; Ono, Y.; Tomiyama, N. Current Status of Embolic Agents for Liver Tumor Embolization. *Int. J. Clin. Oncol.* **2012**, *17*, 306−315.
(14) Seo, K. D.; Kim, D. S. Microfluidic Synthesis of Thermo-Responsive Poly (N-isopropylacrylamide)-Poly (ethylene glycol)

DOI: 10.1021/acsami.7b14330
ACS Appl. Mater. Interfaces 2017, 9, 43478−43489

Diacrylate Microhydrogels as Chemo-Embolic Microspheres. *J. Micromech. Microeng.* **2014**, *24*, 085001.
(15) Derdeyn, C. P.; Moran, C. J.; Cross, D. T.; Dietrich, H. H.; Dacey, R. G. Polyvinyl Alcohol Particle Size and Suspension Characteristics. *American journal of neuroradiology* **1995**, *16*, 1335−1343.
(16) Ma, G. H.; Su, Z. G. Microspheres and Microcapsules in Biotechnology: Design, Preparation and Applications; Pan Stanford Publishing: Singapore, 2013.
(17) Kirchhoff, T. D.; Bleck, J. S.; Dettmer, A.; Chavan, A.; Rosenthal, H.; Merkesdal, S.; Frericks, B.; Zender, L.; Malek, N. P.; Greten, T. F.; Kubicka, S.; Manns, M. P.; Galanski, M. Transarterial Chemoembolization Using Degradable Starch Microspheres and Iodized Oil in the Treatment of Advanced Hepatocellular Carcinoma: Evaluation of Tumor Response, Toxicity, and Survival. *Hepatobiliary Pancreatic Dis. Int.* **2007**, *6*, 259−266.
(18) Weng, L.; Rostamzadeh, P.; Nooryshokry, N.; Le, H. C.; Golzarian, J. In Vitro and In Vivo Evaluation of Biodegradable Embolic Microspheres with Tunable Anticancer Drug Release. *Acta Biomater.* **2013**, *9*, 6823−6833.
(19) Kettenbach, J.; Stadler, A.; Katzler, I.; Schernthaner, R.; Blum, M.; Lammer, J.; Rand, T. Drug-Loaded Microspheres for the Treatment of Liver Cancer: Review of Current Results. *CardioVascular and Interventional Radiology* **2008**, *31*, 468−476.
(20) Shah, R. R.; Davis, T. P.; Glover, A.L.; Nikles, D. E.; Brazel, C. S. Impact of Magnetic Field Parameters and Iron Oxide Nanoparticle Properties on Heat Generation for Use in Magnetic Hyperthermia. *J. Magn. Magn. Mater.* **2015**, *387*, 96−106.
(21) Kolosnjaj-Tabi, J.; Wilhelm, C. Magnetic Nanoparticles in Cancer Therapy: How Can Thermal Approaches Help? *Nanomedicine* **2017**, *12*, 573−575.
(22) Ho, D.; Sun, X.; Sun, S. Monodisperse Magnetic Nanoparticles for Theranostic Applications. *Acc. Chem. Res.* **2011**, *44*, 875−882.
(23) Xie, J.; Zhang, Y.; Yan, C.; Song, L.; Wen, S.; Zang, F.; Yan, C.; Gu, N.; Chen, G.; Ding, Q. High-Performance PEGylated Mn-Zn Ferrite Nanocrystals as a Passive-Targeted Agent for Magnetically Induced Cancer Theranostics. *Biomaterials* **2014**, *35*, 9126−9136.
(24) Yu, H.; Zhu, G. Y.; Xu, R. Z.; Niu, H. Z.; Lu, Q.; Li, G. Z.; Wang, Z. Y.; Zhang, D. S.; Gu, N.; Teng, G. J. Arterial Embolization Hyperthermia Using As_2O_3 Nanoparticles in VX_2 Carcinoma-Induced Liver Tumors. *PLoS One* **2011**, *6*, e17926.
(25) Fan, T.; Wang, X.; Zhou, Y. Targeted Hyperthermia After Selective Embolization with Ferromagnetic Nanoparticles in a VX_2 Rabbit Liver Tumor Model. *Int. J. Nanomed.* **2013**, *8*, 3795−3804.
(26) Gupta, S.; Wright, K. C.; Ensor, J.; Van Pelt, C. S.; Dixon, K. A.; Kundra, V. Hepatic Arterial eEmbolization with Doxorubicin-Loaded Superabsorbent Polymer Microspheres in a Rabbit Liver Tumor Model. *Cardiovascular and interventional radiology* **2011**, *34*, 1021−1030.
(27) Fang, K.; Song, L.; Gu, Z.; Yang, F.; Zhang, Y.; Gu, N. Magnetic Field Activated Drug Release System Based on Magnetic PLGA Microspheres for Chemo-Thermal Therapy. *Colloids Surf., B* **2015**, *136*, 712−720.
(28) Li, X. Q.; Li, Q.; Gong, F. L.; Lei, J. D.; Zhao, X.; Ma, G. H.; Su, Z. G. Preparation of Large-Sized Highly Uniform AgaroseBeads by Novel Rotating Membrane Emulsification. *J. Membr. Sci.* **2015**, *476*, 30−39.
(29) Liang, Y. J.; Fan, F. G.; Ma, M.; Sun, J. F.; Chen, J.; Zhang, Y.; Gu, N. Size-Dependent Electromagnetic Properties and the Related Simulations of Fe_3O_4 Nanoparticles Made by Microwave-Assisted Thermal Decomposition. *Colloids Surf., A* **2017**, *530*, 191−199.
(30) Harvey, J. A. E.; Smart, J. A.; Amis, E. S. Simultaneous Spectrophotometric Determination of Iron (II) and Total Iron with 1, 10-Phenanthroline. *Anal. Chem.* **1955**, *27*, 26−29.
(31) Mornet, S.; Vasseur, S.; Grasset, F.; Duguet, E. Magnetic Nanoparticle Design for Medical Diagnosis and Therapy. *J. Mater. Chem.* **2004**, *14*, 2161−2175.
(32) He, Q.; Zhang, J.; Shi, J.; Zhu, Z.; Zhang, L.; Bu, W.; Guo, L.; Chen, Y. The Effect of PEGylation of Mesoporous Silica Nanoparticles on Nonspecific Binding of Serum Proteins and Cellular Responses. *Biomaterials* **2010**, *31*, 1085−1092.
(33) Chen, J. H.; Lin, Y. C.; Huang, Y. S.; Chen, T. J.; Lin, W. Y.; Han, K. W. Induction of VX_2 Carcinoma in Rabbit Liver: Comparison of Two Inoculation Method. *Lab. Anim.* **2004**, *38*, 79−84.
(34) Earle, J. S. L.; Luthra, R.; Romans, A.; Ensor, J.; Yao, H.; Hamilton, S. R.; Abraham, R. Association of microRNA Expression with Microsatellite Instability Status in Colorectal Adenocarcinoma. *J. Mol. Diagn.* **2010**, *12*, 433−440.
(35) Kumar, M. N. V. R.; Bakowsky, U.; Lehr, C. M. Preparation and Characterization of Cationic PLGA Nanospheres as DNA Carriers. *Biomaterials* **2004**, *25*, 1771−1777.
(36) Xie, J.; Xu, C.; Kohler, N.; Hou, Y.; Sun, S. Controlled PEGylation of Monodisperse Fe_3O_4 Nanoparticles for Reduced Non-specific Uptake by Macrophage Cells. *Adv. Mater.* **2007**, *19*, 3163−3166.
(37) Poli, D.; Manini, P.; Andreoli, R.; Franchini, I.; Mutti, A. Determination of Dichloromethane, Trichloroethylene and Perchloroethylene in Urine Samples by Headspace Solid Phase Microextraction Gas Chromatography-mass Spectrometry. *J. Chromatogr. B: Anal. Technol. Biomed. Life Sci.* **2005**, *820*, 95−102.
(38) Witschi, C.; Doelker, E. Residual Solvents in Pharmaceutical Products: Acceptable Limits, Influences on Physicochemical Properties, Analytical Methods and Documented Values. *Eur. J. Pharm. Biopharm.* **1997**, *43*, 215−242.
(39) Zhang, H.; Hu, L.; Zhong, Y.; Luo, Y. Preparation of Magnetic Poly (lactic-co-glycolic acid) Microspheres Featuring Monodispersity and Controllable Particle Size Using a Microchannel Device. *Polym. Int.* **2015**, *64*, 1425−1432.
(40) Zhang, H.; Deng, J.; Wu, Y. Biobased Magnetic Microspheres Containing Aldehyde Groups: Constructed by Vanillin-Derived Polymethacrylate/Fe3O4 and Recycled in Adsorbing Amine. *ACS Sustainable Chem. Eng.* **2017**, *5*, 658−666.
(41) Shete, P. B.; Patil, R. M.; Thorat, N. D.; Prasad, A.; Ningthoujam, R. S.; Ghosh, S. J.; Pawar, S. H. Magnetic Chitosan Nanocomposite for Hyperthermia Therapy Application: Preparation, Characterization and in Vitro Experiments. *Appl. Surf. Sci.* **2014**, *288*, 149−157.
(42) Verma, M. S.; Liu, S.; Chen, Y. Y.; Meerasa, A.; Gu, F. X. Size-Tunable Nanoparticles Composed of Dextran-b-poly (D, L-lactide) for Drug Delivery Applications. *Nano Res.* **2012**, *5*, 49−61.
(43) Moroz, P.; Jones, S. K.; Winter, J.; Gray, B. N. Targeting Liver Tumors with Hyperthermia: Ferromagnetic Embolization in a Rabbit Liver Tumor Model. *J. Surg. Oncol.* **2001**, *78*, 22−29.
(44) Yan, S.; Zhang, D.; Gu, N.; Zheng, J.; Ding, A.; Wang, Z.; Xing, B.; Ma, M.; Zhang, Y. Therapeutic Effect of Fe_2O_3 Nanoparticles Combined with Magnetic Fluid Hyperthermia on Cultured Liver Cancer Cells and Xenograft Liver Cancers. *J. Nanosci. Nanotechnol.* **2005**, *5*, 1185−1192.
(45) Du, L.; Zhou, J.; Wang, X.; Sheng, L.; Wang, G.; Zhao, L.; Liao, Y.; Tang, J.; Xie, X.; Xu, G. Effect of Local Hyperthermia Induced by Nanometer Magnetic Fluid on the Rabbit VX_2 Liver Tumor Model. *Prog. Nat. Sci.* **2009**, *19*, 1705−1712.
(46) Hedayatnasab, Z.; Abnisa, F.; Daud, W. M. A. W. Review on Magnetic Nanoparticles for Magnetic Nano-fluid Hyperthermia Application. *Mater. Des.* **2017**, *123*, 174−196.
(47) Geschwind, J. F. H.; Ko, Y. H.; Torbenson, M. S.; Magee, C.; Pedersen, P. L. Novel Therapy for Liver Cancer. *Cancer Res.* **2002**, *62*, 3909−3913.
(48) Storm, F. K.; Harrison, W. H.; Elliott, R. S.; Morton, D. L. Normal Tissue and Solid Tumor Effects of Hyperthermia in Animal Models and Clinical Trials. *Cancer Res.* **1979**, *39*, 2245−2251.
(49) Sanz, B.; Calatayud, M. P.; Torres, T. E.; Fanarraga, M. L.; Ibarra, M.; Goya, G. F. Magnetic Hyperthermia Enhances Cell Toxicity with Respect to Exogenous Heating. *Biomaterials* **2017**, *114*, 62−70.
(50) Schroeder, A.; Heller, D. A.; Winslow, M. M.; Dahlman, J. E.; Pratt, G. W.; Langer, R.; Jacks, T.; Anderson, D. G. Treating

DOI: 10.1021/acsami.7b14330
ACS Appl. Mater. Interfaces 2017, 9, 43478−43489

Metastatic Cancer with Nanotechnology. *Nat. Rev. Cancer* **2011**, *12*, 39−50.
(51) Vousden, K. H.; Lu, X. Live or Let Die: The Cell's Response to p53. *Nat. Rev. Cancer* **2002**, *2*, 594−604.
(52) Liu, L. L.; Fu, D.; Ma, Y.; Shen, X. Z. The Power and the Promise of Liver Cancer Stem Cell Markers. *Stem Cells Dev.* **2011**, *20*, 2023−2030.
(53) Zhou, Y.; Gao, J. B.; Xu, H.; Dong, J.; Wang, M. Y. Evaluation of Neovascularization with Spectral Computed Tomography in a Rabbit VX_2 Liver Model: a Comparison with Real-Time Contrast-Enhanced Ultrasound and Molecular Biological Findings. *Br. J. Radiol.* **2015**, *88*, 20140548.
(54) Lindahl, R. Aldehyde Dehydrogenases and Their Role in Carcinogenesis. *Crit. Rev. Biochem. Mol. Biol.* **1992**, *27*, 283−335.
(55) Jiang, H. J.; Lu, H. B.; Zhang, Z. R.; Wang, Y. M.; Huang, Q.; Huang, Y. H.; Li, J. P.; Shu, S. J.; Wang, J. E. Experimental Study on Angiogenesis in a Rabbit VX_2 Early Liver Tumor by Perfusion Computed Tomography. *J. Int. Med. Res.* **2010**, *38*, 929−939.
(56) Goldenberg, D.; Ayesh, S.; Schneider, T.; Pappo, O.; Jurim, O.; Eid, A.; Fellig, Y.; Dadon, T.; Ariel, I.; de Groot, N.; Hochberg, A.; Galun, E. Analysis of Differentially Expressed Genes in Hepatocellular Carcinoma using cDNA Arrays. *Mol. Carcinog.* **2002**, *33*, 113−124.
(57) Levine, A. J.; Momand, J.; Finlay, C. A. The p53 Tumor Suppressor Gene. *Nature* **1991**, *351*, 453.
(58) Guan, J.; Stavridi, E.; Leeper, D. B.; Iliakis, G. Effects of Hyperthermia on p53 Protein Expression and Activity. *J. Cell. Physiol.* **2002**, *190*, 365−374.
(59) Gehlot, P.; Shukla, V.; Gupta, S.; Makidon, P. E. Detection of ALDH1 Activity in Rabbit Hepatic VX_2 Tumors and Isolation of ALDH1 Positive Cancer Stem Cells. *J. Transl. Med.* **2016**, *14*, 49.
(60) Hanahan, D.; Folkman, J. Patterns and Emerging Mechanisms of the Angiogenic Switch During Tumorigenesis. *Cell* **1996**, *86*, 353−364.
(61) Stel, V. S.; Dekker, F. W.; Tripepi, G.; Zoccali, C.; Jager, K. J. Survival Analysis I: the Kaplan-Meier Method. *Nephron J.* **2011**, *119*, c83−c88.

DOI: 10.1021/acsami.7b14330
ACS Appl. Mater. Interfaces 2017, 9, 43478−43489